Single Image Dehazing Using Color Ellipsoid Prior

Trung Minh Bui, *Student Member, IEEE*, and Wonha Kim, *Senior Member, IEEE*

***Abstract*— In this paper, we propose a new single-image dehazing method. The proposed method constructs color ellipsoids that are statistically fitted to haze pixel clusters in RGB space and then calculates the transmission values through color ellipsoid geometry. The transmission values generated by the proposed method maximize the contrast of dehazed pixels, while preventing over-saturated pixels. The values are also statistically robust because they are calculated from the averages of the haze pixel values. Furthermore, rather than apply a highly complex refinement process to reduce halo or unnatural artifacts, we embed a fuzzy segmentation process into the construction of the color ellipsoid so that the proposed method simultaneously executes the transmission calculation and the refinement process. The results of an experimental performance evaluation verify that compared with prevailing dehazing methods the proposed method performs effectively across a wide range of haze and noise levels without causing any visible artifacts. Moreover, the relatively low complexity of the proposed method will facilitate its real-time applications.**

***Index Terms*— Dehazing, dark channel prior (DCP), color ellipsoid prior (CEP).**

I. Introduction

MANY competitive single-image dehazing methods are based on the dichromatic model [1]–[9], which describes a hazy image as a mixture of the transmitted portion of the haze-free image and the portion of the light source that reaches the camera. Describing the dichromatic model in the RGB color space, the vectors of the hazier pixels are the more densely clustered. The dehazing methods based on the dichromatic model select a vector to indicate the extent to which pixel colors are diluted or hazed by the atmospheric light; that vector is named the prior vector. The prior vector could be selected from pixels [2], [3], [5], [9] or it could be calculated from the geometry of cluster distributions [1], [4], [6]. Those methods then linearly stretch the hazy vector cluster from the atmospheric light to each hazy vector until any color components of the stretched prior vector become zeros [2]–[4] or the stretched prior vector reaches to the origin [1], [6]. Thus, the selection of the prior vector determines the accuracy of transmission estimation and thereby the dehazing performance.

Manuscript received March 7, 2016; revised December 3, 2016 and April 1, 2017; accepted October 24, 2017. Date of publication November 8, 2017; date of current version November 28, 2017. This work was supported in part by the Korean Minister of Industry under Grant 10052967 and in part by the National Research Foundation of Korea under Grant NRF-2015R1D1A1A01059722. The associate editor coordinating the review of this manuscript and approving it for publication was Dr. Hamid R. Sheikh. *(Corresponding author: Wonha Kim.)*

The authors are with the College of Electronics and Information, Kyung Hee University, Yongin 17104, South Korea (e-mail: wonha@khu.ac.kr).

Color versions of one or more of the figures in this paper are available online at http://ieeexplore.ieee.org.

Digital Object Identifier 10.1109/TIP.2017.2771158

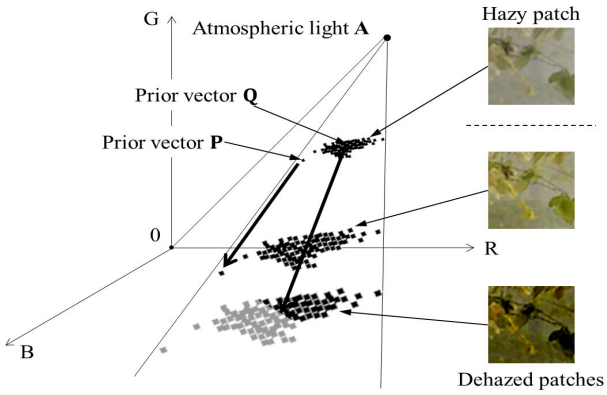

Fig. 1. Dehazing results by different prior vectors. The gray dots illustrate the over-saturated pixel vectors.

When selecting the prior vector, its location, the randomness of the image signal, and the homogeneity of the image signal are all important factors.

Fig. 1 illustrates different dehazings with different prior vectors and shows the dehazing results. The prior vector **P** expands the hazy vector distribution less than the prior vector **Q**, which means that the image dehazed by the prior vector **P** retains natural saturation but has lower contrast, while the one dehazed by the prior vector **Q** has higher contrast but also has the possibility of producing over-saturation, which usually appears as dark spots. To strike a balance between these results, each method for estimating transmission tries to set its prior vector location to maximize the contrast of dehazed images while suppressing the over-saturation.

Because image signals are random, the signals from a local region may include irregular pixels that are rarely correlated with the majority of pixels of the underlying local image. Fig. 2 shows the distribution of pixel values for two nearby regions in a hazy image. Even if one region includes the irregular pixels that appear as small dark spots, these two proximate regions exhibit similar overall characteristics and equivalent degrees of haziness. However, when the prior vector is selected from among the irregular pixels, the dehazing result is insufficient because the prior vector is irrelevant to the majority of pixels and is closer to the origin. Therefore, the selection of the prior vector must also be statistically robust against signal randomness.

In a region across different objects, the vector cluster is combined from those objects, and so there exist multiple prior vectors that are appropriate for each object region. Fig. 3 illustrates the color vector distribution of a region that spans two different objects. There are two prior vector candidates: vectors **P** matching the leaves, and **Q** matching the deep forest. A prior vector selected from the mixed pixel vector distribution

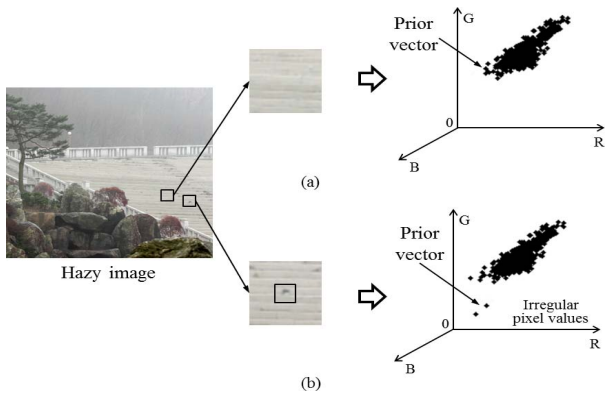

Fig. 2. Pixel value distributions of two nearby regions and their expected prior vectors. (a) Region without irregularly dark pixels, (b) region with irregular pixels.

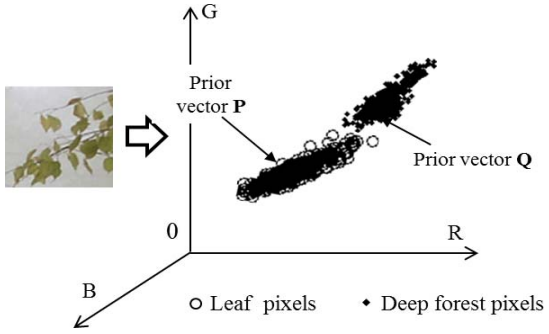

Fig. 3. Vector distribution of image patch including different regions, and the prior vector candidates.

of the two object regions often produces a mismatch with one of the object regions, resulting in a halo artifact apparent along the strong edges [2], [4]. Alternatively, instead of selecting a prior vector from the mixed distribution of the heterogeneous region, the prior vector could be interpolated from prior vectors of neighboring homogeneous regions. However, the interpolated vector may not be relevant enough to the pixel vector distribution and may cause insufficient or excessive dehazing results [6].

In order to compensate for the mismatched or erroneous selections of prior vectors, an additional post-refinement process is required. Methods in [2], [5], and [10] smooth out abrupt transmission transitions by soft-matting, contextual regularization, or guided filtering. In [6] and [9], the Gauss-Markov random field model was adopted to regularize the interpolated transmission values. Most of these refinement methods cost an additional computational load that is heavier than those of the transmission estimation processes themselves, thereby limiting their application in actual dehazing systems.

A well-known local dehazing method in [2] selects the prior vector from the pixel having the minimum color component value in the image region. The method in [5] similarly selects the prior vector and adds a lower bound to limit the cluster stretch. Other methods in [3] and [4] select the medium vector of a vector cluster, which usually excessively stretches the hazy vector cluster and often results in over-saturation. Berman *et al.* [9] proposed the non-local method, by which whole pixel values are classified into color clusters. For each cluster, the vector farthest from the atmospheric light is selected as the prior vector. Unlike the methods for selecting a pixel value as the prior vector, Fattal proposes a statistical color-line fitting method [6], in which a line supported by the majority of pixels is constructed, and the prior vector is calculated from the intersection between the atmospheric light and the constructed line. The learning-based methods in [7] and [8] directly estimate the transmission values through a learning procedure. In the specific cases matching training datasets, these methods may produce better performance. However, because they use pure white atmospheric light in the training process, the performance of these methods quickly decreases when atmospheric light is chromatic [11].

The methods in [12] and [13] employ contrast enhancement, rather than models, to increase the visibility of images. These methods have been reported to exhibit inferior performance compared to the model-based methods.

In this paper, we propose a dichromatic, model-based dehazing method that is statistically robust against image signal randomness, performs effectively across a wide range of haze degrees, does not require any post-refinement process, and does not produce any apparently visible noise or halo artifacts. For statistical robustness, we fit the pixel vector cluster in RGB space to a statistical color ellipsoid constructed from the moments of the pixel values. Instead of selecting a pixel for the prior vector, the proposed method calculates the prior vector using ellipsoid geometry. The calculated prior vector has the minimum color component among the vectors on the ellipsoid surface in order to maximize the contrast of the dehazed pixels in any degree of haze where most pixels are not saturated. To avoid the halo artifact, we embed a fuzzy process into the construction of the color ellipsoid, rather than applying highly complex post-processes.

The remainder of this paper is organized as follows: In Section II, we discuss the concerns with the currently prevailing methods. In Section III, we propose a dehazing method based on color ellipsoid prior (CEP). The performance of the proposed dehazing method is discussed in Section IV, and our conclusions are presented in Section V.

II. Revisit to Existing Dehazing Methods

In this section, we investigate three methods of [2], [6], and [9] that are reported to produce competitive performances [11]. We analyze how each method selects the prior vector in RGB space and discuss the issues with each method.

The dichromatic model recovers the haze-free image $\tilde{\mathbf{x}}_i$ from the hazy image $\mathbf{x}_i$ at the location of i such that [2], [6], [9],

$$\mathbf{x}_i = t_i \cdot \tilde{\mathbf{x}}_i + (1 - t_i) \cdot \mathbf{A} \tag{1}$$

where $\mathbf{A} = [A_r \ A_g \ A_b]^T$ is the global atmospheric light, and t_i is the transmission value; t_i is determined by a prior value extracted from a prior vector. In view of the RGB space, dehazing methods based on the dichromatic model linearly stretch the hazy vectors at a ratio of $1/t_i$ along the line

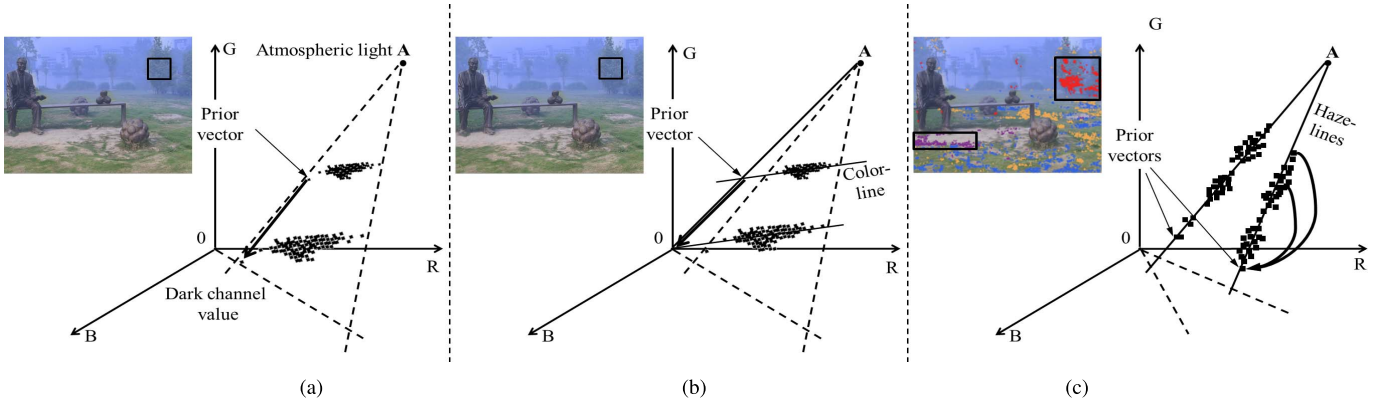

Fig. 4. Dehazing procedures in RGB space. (a) Dehazing by the DCP [2], (b) by the color-line [6], and (c) by the haze-line [9].

from the atmospheric light to each hazy vector. Each dehazing method selects its own prior vector and then extracts its own prior value from that vector.

Fig. 4 illustrates how the dehazing methods in [2], [6], and [9] select the prior vectors and stretch the hazy vector clusters. In Fig. 4(a), by observing that the minimum color components of haze-free patches are sufficiently small that they approach zero, He *et al.* selected the pixel having the minimum color component to determine the prior vector, and stretched the hazy vectors until any color component of the stretched prior vectors reached zero. The minimum color component is called the dark channel value, and the method is named the dark channel prior (DCP) [2]. The DCP performs effectively at a variety of haze levels. However, because the method always searches for the minimum color component; so in regions that include tiny sporadic dark textures, the method selects the prior vector from these dark pixels, which are almost irrelevant to the majority of pixels. The prior vector from the dark pixels often does not stretch the hazy vector clusters sufficiently, resulting in a dehazed image that remains hazy. Therefore, the issue with this method is its statistical instability against the randomness of image signals. In heterogeneous regions, because the DCP selects a prior vector that cannot match all of the vector groups from different regions, this method often produces a halo artifact along object boundaries.

Fig. 4(b) shows the method proposed by Fattal [6]. Instead of selecting the prior vectors among pixel values, this method calculates the prior vector, assuming from the previous works [14], [15] that most pixels within a small haze-free patch are mono-chromatic to support a color line passing through the origin. This method also assumes that the color lines in the hazy patches are shifted from the origin by the contributions of atmospheric light. The method statistically constructs the color line from the majority of pixels in small hazy patches, for example 7×7, and selects the prior vector of the patch as that which intersects the color line and the atmospheric light. With well-constructed color lines, the method can achieve a natural haze-free image. However, because the mono-chromatic assumption holds only for small patches, the statistics from a small number of pixels may not be reliable in regions with low variation, which are often caused by dense haze or high noise levels. In order to avoid unreliable prior vectors, the color-line method discards prior vectors for patches not obeying the assumption, and then interpolates the discarded prior vectors from neighboring valid prior vectors. The issues with this approach are that the valid prior vectors in the heavy haze areas may not be sufficient to interpolate the discarded prior vectors, and the decision criteria for discarding the invalid prior vectors are also incomplete. Therefore, this method may result in insufficient or erroneous dehazing in heavy haze regions.

Fig. 4(c) presents the method of [9]. Berman *et al.* used a non-local method. They classified all hazy image pixels into, at maximum, 500 color clusters, then assigned a prior vector to each cluster such that the vector is farthest from the atmospheric light of each cluster. The vector clusters tend to be distributed along the lines elongated from the prior vectors of each clusters toward the atmospheric light, called the haze lines. Referred to as the haze-line approach, this method assumes that the prior vectors are haze-free, and stretches the hazy vectors along each haze line until each stretched vector is close to the corresponding prior vectors. This non-local approach working on each pixel is well adapted to the details, and therefore achieves good transmission estimation at certain hazy levels. However, as the hazy level increases, the classification accuracies inherently decrease, and the assumption that the prior vectors should be haze-free becomes less valid, so that the haze-line method is insufficient for reducing haze at heavy haze levels. Additionally, although the non-local approach does not cause mismatch prior vectors, it may cause over-saturation, which widens the dark regions usually associated with thin objects against a heavy haze background.

III. Color Ellipsoid Prior Method

In this section, we develop the dehazing method adopting the statistical ellipsoid fitting method. The developed method is statistically robust against signal randomness, performs effectively across a wide range of haze degrees, does not require any post-refinement processing, and does not produce any visible noise or halo artifacts. The method derives the prior vector to have the minimum color component on the color ellipsoid surface.

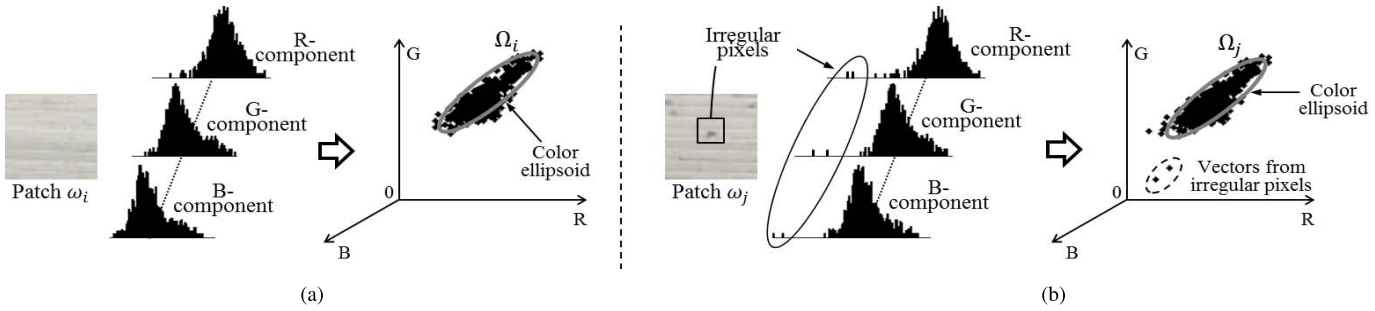

Fig. 5. Statistical color ellipsoid constructions of two nearby patches. The patch images are similar in overall characteristics. (a) Ellipsoid construction of the region without irregular pixels, (b) with irregular pixels. Two ellipsoids, $\mathbf{\Omega}_i$ and $\mathbf{\Omega}_j$ are almost same, whereas the distributions of pixels in ω_i and ω_j are different.

A. Color Ellipsoid Prior (CEP)

In the RGB color space, the vectors from hazier image signals are more densely clustered and normally distributed [4], [16]. The vector cluster region can be statistically approximated by an ellipsoid, where the shape of the ellipsoid is determined by the statistical moments of the vector distribution. An advantage of analyzing the ellipsoid is that it provides statistical robustness against random signals.

We denote $\mathbf{z} = [z_r \ z_g \ z_b]^T$ as a vector variable in the RGB space. Let $\mathbf{\Omega}_i$ be the ellipsoid that fits the vector cluster region of the color pixels in ω_i. Then, $\mathbf{\Omega}_i$ can be constructed in the following manner [4]:

$$\Omega_i = \left\{ \mathbf{z} \mid (\mathbf{z} - \boldsymbol{\mu}_i)^T \mathbf{\Sigma}_i^{-1} (\mathbf{z} - \boldsymbol{\mu}_i) \leq 1 \right\}, \tag{2}$$

where

$$\text{normalized pixel}: \quad \bar{\mathbf{x}}_j = \left[\frac{x_{r,j}}{A_r} \ \frac{x_{g,j}}{A_g} \ \frac{x_{b,j}}{A_b} \right]^T,$$

$$\text{mean vector}: \quad \boldsymbol{\mu}_i = \frac{1}{|\omega_i|} \sum_{j \in \omega_i} \bar{\mathbf{x}}_j = [\mu_{r,i} \ \mu_{g,i} \ \mu_{b,i}]^T,$$

$$\text{covariance matrix}: \quad \mathbf{\Sigma}_i = \frac{1}{|\omega_i|} \sum_{j \in \omega_i} (\bar{\mathbf{x}}_j - \boldsymbol{\mu})(\bar{\mathbf{x}}_j - \boldsymbol{\mu})^T$$

$$= \begin{bmatrix} \sigma_{r,i}^2 & \sigma_{rg,i} & \sigma_{rb,i} \\ \sigma_{gr,i} & \sigma_{g,i}^2 & \sigma_{gb,i} \\ \sigma_{br,i} & \sigma_{bg} & \sigma_{b,i}^2 \end{bmatrix}.$$

In the RGB space, $\boldsymbol{\mu}_i$ is located at the ellipsoid center, and $\mathbf{\Sigma}_i$ determines the shape and orientation of the ellipsoid.

Fig. 5 depicts the construction of statistical ellipsoids for two nearby patches. Even if one patch includes irregular pixels, the two proximate patches have similar characteristics and equivalent degrees of haziness. The ellipsoids are built from the statistical averages, so the irregular vectors from noise or sporadic textures, which are rarely correlated with the overall distribution, are averaged away and have little effect on the shape of the ellipsoid. Thus, the ellipsoids are equivalent regardless of irregular pixels. This indicates that the analysis based on the ellipsoids is more robust than the analysis based on the pixel values.

The proposed method calculates the vector having the smallest color component among the vectors in the ellipsoid $\mathbf{\Omega}_i$ to maximally stretch the hazy vector cluster while preventing the color components of the majority of stretched vectors from being negative. Thus, the proposed method fully dehazes the image without presenting the saturated pixels as dark spots. We call this prior vector the color ellipsoid prior (CEP) vector. Then, the CEP value is calculated as follows:

$$\theta_i = \min_{\mathbf{z} \in \mathbf{\Omega}_i} \left\{ \min_{c \in \{r,g,b\}} z_c \right\}, \tag{3}$$

Hereinafter, we calculate the CEP value θ_i directly from the ellipsoid geometry. We will drop the location subscript i for clarity. Let each unit color component vector be $\mathbf{e}_r = [1 \ 0 \ 0]^T$, $\mathbf{e}_g = [0 \ 1 \ 0]^T$ and $\mathbf{e}_b = [0 \ 0 \ 1]^T$. Denote $\mathbf{H}_c$ for the plane perpendicular to the unit vector $\mathbf{e}_c$ ($c \in \{r, g, b\}$) and passing through the origin. Then, $z_c = \mathbf{e}_c^T \mathbf{z}$ is c-component value of $\mathbf{z}$ and also the distance from $\mathbf{z}$ to $\mathbf{H}_c$. Let $\mathbf{z}_c^*$ be the vector minimizing the distance $\mathbf{e}_c^T \mathbf{z}$, that is, $\min_{\mathbf{z} \in \mathbf{\Omega}_i} \left\{ \mathbf{e}_c^T \mathbf{z} \right\} = \mathbf{e}_c^T \mathbf{z}_c^*$. Fig. 6 depicts the geometry of $\mathbf{z}_r^*$, $\mathbf{z}_g^*$, and $\mathbf{z}_b^*$, which are closest to the $\mathbf{H}_r$, $\mathbf{H}_g$, $\mathbf{H}_b$ planes, respectively.

The $\mathbf{z}_c^*$ closest to the plane $\mathbf{H}_c$ is easily shown to be on the surface of $\mathbf{\Omega}_i$. Then, considering that the vectors on the surface of the ellipse satisfy $S(\mathbf{z}) = (\mathbf{z} - \boldsymbol{\mu})^T \mathbf{\Sigma}^{-1} (\mathbf{z} - \boldsymbol{\mu}) = 1$, the CEP value in (3) can be determined as follows:

$$\theta_i = \min_{\mathbf{z} \in \mathbf{\Omega}_i} \left\{ \min_{c \in \{r,g,b\}} z_c \right\} = \min_{c \in \{r,g,b\}} \left\{ \min_{\mathbf{z} \in \mathbf{\Omega}_i} \{ \mathbf{e}_c^T \mathbf{z} \} \right\}$$

$$= \min_{c \in \{r,g,b\}} \{ \mathbf{e}_c^T \mathbf{z}_c^* \},$$

$$\text{where} \quad S(\mathbf{z}_c^*) = (\mathbf{z}_c^* - \boldsymbol{\mu})^T \mathbf{\Sigma}^{-1} (\mathbf{z}_c^* - \boldsymbol{\mu}) = 1. \tag{4}$$

As seen in Fig. 6, for $\mathbf{z}_c^*$ to be closest to $\mathbf{H}_c$, the plane tangent to the ellipse surface at $\mathbf{z}_c^*$ must be parallel with $\mathbf{H}_c$. Therefore, the outward normal vector of the ellipse surface at $\mathbf{z}_c^*$ is $-\mathbf{e}_c$ [17]. The gradient direction of a vector on the ellipse surface is perpendicular to the tangent plane, and hence the outward normal vector must have the same direction as the gradient of the ellipse surface. Thus, As seen in Fig. 6, in order for $\mathbf{z}_c^*$ to be closest to $\mathbf{H}_c$, the plane tangent to the ellipse surface at $\mathbf{z}_c^*$ must be parallel to $\mathbf{H}_c$. So, the outward normal vector of the ellipse surface at $\mathbf{z}_c^*$ is $-\mathbf{e}_c$ [17]. The gradient direction of a vector on the ellipse surface is perpendicular to the tangent plane, and so the outward normal vector must have the same direction as the gradient of the ellipse surface.

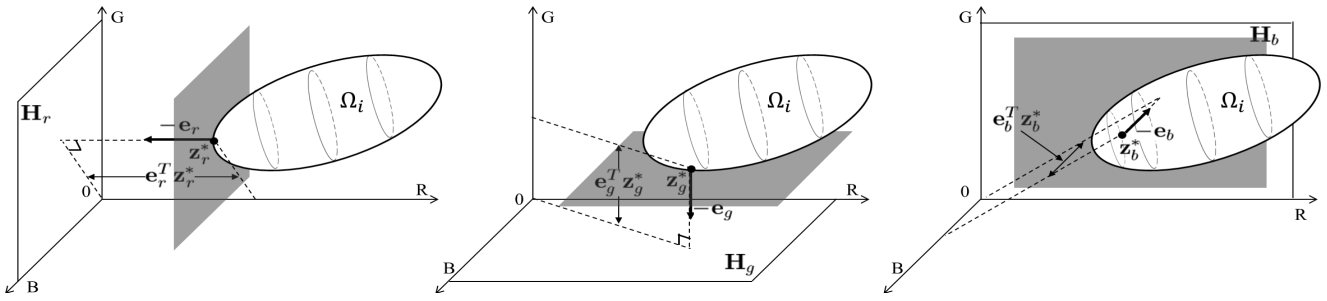

Fig. 6. Geometry of vectors closest to each coordinate plane. (a) Vector $\mathbf{z}_r^*$ is the closest to the B-G plane ($\mathbf{H}_r$). The shadow plane is tangent to ellipsoid surface. The plane is parallel with $\mathbf{H}_r$. $\mathbf{e}_r^T\mathbf{z}_r^*$ is distance from $\mathbf{z}_r^*$ to $\mathbf{H}_r$. (b) $\mathbf{z}_g^*$ is the closest to the B-R plane ($\mathbf{H}_g$). (c) $\mathbf{z}_b^*$ is the closest to the R-G plane ($\mathbf{H}_b$).

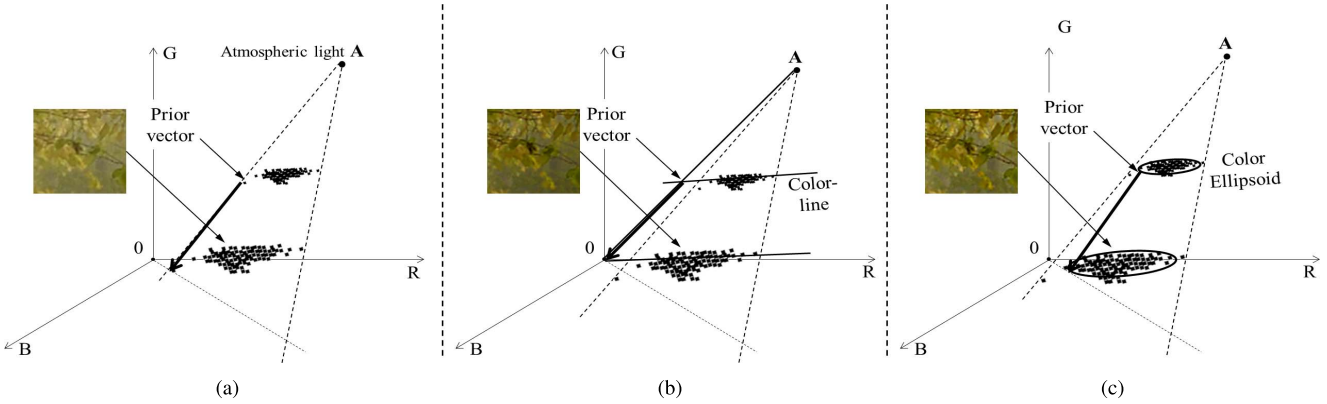

Fig. 7. Comparison of local dehazing procedures. (a) Dehazing by the DCP, (b) by the color-line, and (c) by the proposed CEP.

Thus,

$$\frac{\nabla_{\mathbf{z}} S(\mathbf{z}_c^*)}{\|\nabla_{\mathbf{z}} S(\mathbf{z}_c^*)\|} = -\mathbf{e}_c,$$

where the gradient is computed as [17]

$$\begin{aligned}\nabla_{\mathbf{z}} S(\mathbf{z}_c^*) &= \frac{d}{d\mathbf{z}}\left\{(\mathbf{z}-\boldsymbol{\mu})^T\boldsymbol{\Sigma}^{-1}(\mathbf{z}-\boldsymbol{\mu})\right\}|_{\mathbf{z}=\mathbf{z}_c^*} \\ &= 2\Sigma^{-1}(\mathbf{z}_c^*-\boldsymbol{\mu}).\end{aligned}$$

By replacing $\nabla_{\mathbf{z}} S(\mathbf{z}_c^*)$ with $2\Sigma^{-1}(\mathbf{z}_c^*-\boldsymbol{\mu})$,

$$\mathbf{z}_c^* - \boldsymbol{\mu} = -\boldsymbol{\Sigma}\mathbf{e}_c\|\boldsymbol{\Sigma}^{-1}(\mathbf{z}_c^*-\boldsymbol{\mu})\|. \tag{5}$$

Then,

$$\begin{aligned}S(\mathbf{z}_c^*) &= (\mathbf{z}_c^*-\boldsymbol{\mu})^T\boldsymbol{\Sigma}^{-1}(\mathbf{z}_c^*-\boldsymbol{\mu}) \\ &= (\boldsymbol{\Sigma}\mathbf{e}_c\|\boldsymbol{\Sigma}^{-1}(\mathbf{z}_c^*-\boldsymbol{\mu})\|)^T\boldsymbol{\Sigma}^{-1}(\boldsymbol{\Sigma}\mathbf{e}_c\|\boldsymbol{\Sigma}^{-1}(\mathbf{z}_c^*-\boldsymbol{\mu})\|) \\ \text{since } \boldsymbol{\Sigma}^T &= \boldsymbol{\Sigma}, \\ &= \|\boldsymbol{\Sigma}^{-1}(\mathbf{z}_c^*-\boldsymbol{\mu})\|^2\mathbf{e}_c^T\boldsymbol{\Sigma}\mathbf{e}_c = 1.\end{aligned}$$

This leads to,

$$\|\boldsymbol{\Sigma}^{-1}(\mathbf{z}_c^*-\boldsymbol{\mu})\| = \frac{1}{\sqrt{\mathbf{e}_c^T\boldsymbol{\Sigma}\mathbf{e}_c}} = \frac{1}{\sigma_c}. \tag{6}$$

From (5) and (6), the minimum distance from a vector of Ω_i to plane $\mathbf{H}_c$ is

$$\mathbf{e}_c^T\mathbf{z}_c^* = \mathbf{e}_c^T\left(\boldsymbol{\mu} - \frac{1}{\sigma_c}\Sigma\mathbf{e}_c\right) = \mu_c - \sigma_c. \tag{7}$$

Then, the proposed CEP value is obtained as

$$\theta_i = \min_{c\in\{r,g,b\}}\{\mathbf{e}_c^T\mathbf{z}_c^*\} = \min_{c\in\{r,g,b\}}\{\mu_{c,i} - \sigma_{c,i}\}. \tag{8}$$

Therefore, the CEP transmission estimator becomes

$$t_i = 1 - \alpha\ \theta_i = 1 - \alpha \min_{c\in\{r,g,b\}}\left\{\mu_{c,i} - \sigma_{c,i}\right\}. \tag{9}$$

Fig. 7 compares the dehazing procedures of the local methods. While the DCP method selects the prior vector from the pixels in the patch, the proposed CEP method calculates the prior vector through the statistical color ellipsoid model, for the vector to be statistically robust. Whereas the color-line model is valid only when the image patch size is small enough for the pixel colors to be mono-chromatic, the proposed CEP model does not restrict the patch sizes. Thus, the color ellipsoid constructed by the CEP model is more reliable, and the proposed method enables selection of prior vectors for every pixel.

B. Hallo Artifact Reduction by Fuzzy Segmentation

The work in [18] demonstrates that halo artifacts occur in heterogeneous regions when a pixel selected as a prior vector does not belong to the same region that includes the patch center. Based on the observation, we propose a method that significantly reduces halo artifacts by forcing the location of the prior vector to be in the same vector distribution that includes the patch center pixel vector.

We separate the heterogeneous patch ω_i into a set of foreground pixels ω_i^f and a set of background pixels ω_i^b. Then we

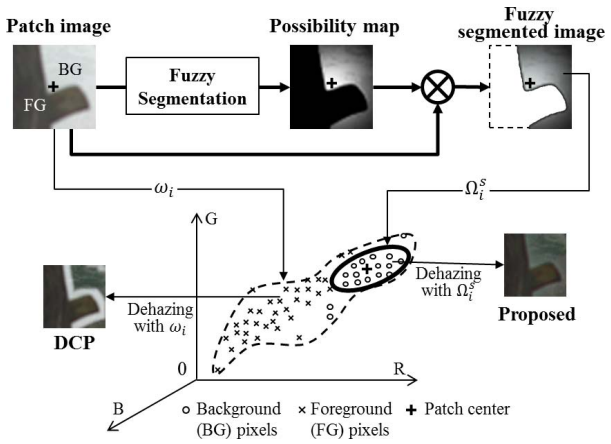

Fig. 8. Ellipsoid construction using fuzzy segmentation at a heterogenous patch.

denote Ω_i^b and Ω_i^f as the statistical ellipsoids constructed by ω_i^b and ω_i^f, respectively. To avoid transmission mismatches, the proposed method constructs the statistical ellipsoids from the pixels only in the region that covers the patch center. The prior value is then obtained in the following manner:

$$\theta_i = \min_{\mathbf{z}\in\Omega_i^s}\left\{\min_{c\in\{r,g,b\}} z_c\right\},$$

$$\text{where}\quad \Omega_i^s = \begin{cases}\Omega_i^b, & \text{if } i \in \omega_i^b\\ \Omega_i^f, & \text{if } i \in \omega_i^f.\end{cases} \tag{10}$$

In order to implement (10), we need to determine whether a pixel belongs to the same region that contains the patch center. The real image boundaries between background and foreground regions are often uncertain, so we use a fuzzy decision method to segment pixel regions by examining the pixel value variations and pixel locations.

We compute the fuzzy decision value by measuring the possibility P_{ij} that the pixel at j is in the region including the patch center at location i. Several filters have been developed for estimating P_{ij} [10], [19]. When the pixel j is in the same region that contains the patch center i, these filters smoothly increase P_{ij} as the distance from the location of the pixel at j to that of the patch center at i decreases. When j is not in the region with the patch center i, the filters let P_{ij} be close to 0. Then, Ω_i^s is constructed from the image pixels filtered using P_{ij}. Thus, the center vector $\hat{\boldsymbol{\mu}}$ and the covariance matrix $\hat{\boldsymbol{\Sigma}}$ used to construct Ω_i^s are calculated as follows:

$$\hat{\boldsymbol{\mu}}_i = \sum_{j\in\omega_i} P_{ij}\bar{\mathbf{x}}_j, \quad \hat{\boldsymbol{\Sigma}}_i = \sum_{j\in\omega_i} P_{ij}(\bar{\mathbf{x}}_j - \hat{\boldsymbol{\mu}}_i)(\bar{\mathbf{x}}_j - \hat{\boldsymbol{\mu}}_i)^T, \tag{11}$$

where $\sum_{j\in\omega_i} P_{ij} = 1$. Then, the CEP transmission estimator embedding fuzzy segmentation becomes

$$t_i = 1 - \alpha \min_{c\in\{r,g,b\}}\left\{\hat{\mu}_{c,i} - \hat{\sigma}_{c,i}\right\}, \tag{12}$$

where $\hat{\mu}_{c,i} = \sum_{j\in\omega_i} P_{ij}\bar{x}_{c,j}$ and $\hat{\sigma}_{c,i}^2 = \sum_{j\in\omega_i} P_{ij}(\bar{x}_{c,j} - \hat{\mu}_{c,i})^2$.

Fig. 8 illustrates the procedure used to construct the ellipsoid with only the pixels in the region at the patch center. The patch center is in the background and marked by a cross. We construct the ellipsoid with the image masked with P_{ij}, where P_{ij} is close to zero in the foreground. Therefore, independent of the boundary uncertainty and region geometries, Ω_i^s is constructed using only the pixels in the background that include the patch center. Referring to the guided filter in [10], we realize P_{ij} with sequential operations of average filters. The detailed implementation is described in Table I.

TABLE I
FAST CEP IMPLEMENTATION WITH GUIDED FILTER SEGMENTATION

Parameters:
Patch center : i, Patch size : $|\omega|$, Regularization : ϵ

Procedures :

- Determine the minimum color component :
  $\bar{x}_{c^*,j} = \min\{\bar{x}_{r,j}, \bar{x}_{g,j}, \bar{x}_{b,j}\}$

• Fuzzy estimation of mean
- Calculate mean and variance:
  $\mu_i = \sum_{j\in\omega_i} \bar{x}_{c^*,j}/|\omega|,\ \sigma_i^2 = \sum_{j\in\omega_i} (\bar{x}_{c^*,j} - \mu_i)^2/|\omega|$
- Calculate fuzzy segmentation strength:
  $a_i = \sigma_i^2/(\sigma_i^2 + \epsilon),\ b_i = (1 - a_i)\mu_i$
  $\bar{a}_i = \sum_{j\in\omega_i} a_j/|\omega|,\quad \bar{b}_i = \sum_{j\in\omega_i} b_j/|\omega|$
- Calculate cluster-classified mean:
  $\hat{\mu}_{c^*,i} = \bar{a}_i\bar{x}_{c^*,i} + \bar{b}_i$

• Fuzzy estimation of variance
- Determine detail layer:
  $d_j = (\bar{x}_{c^*,j} - \hat{\mu}_j)^2$
- Calculate mean and covariance of detail layer:
  $\mu_i^d = \sum_{j\in\omega_i} d_j/|\omega|,$
  $\sigma_i^d = \sum_{j\in\omega_i} (\bar{x}_{c^*,j} - \mu_j)(d_j - \mu_i^d)/|\omega|$
- Calculate fuzzy segmentation strength:
  $k_i = \sigma_i^d/(\sigma_i^2 + \epsilon),\ m_i = (1 - k_i)\mu_i^d$
  $\bar{k}_i = \sum_{j\in\omega_i} k_j/|\omega|,\quad \bar{m}_i = \sum_{j\in\omega_i} m_j/|\omega|$
- Calculate cluster-classified variance:
  $\hat{\sigma}_{c^*,i} = \bar{k}_i\bar{x}_{c^*,i} + \bar{m}_i$

• Determine the transmission value
  $t_i = 1 - \alpha(\hat{\mu}_{c^*,i} - \hat{\sigma}_{c^*,i})$.

Fig. 9 shows images dehazed with and without the fuzzy segmentation. The transmission with no fuzzy segmentation is smooth but not precise at the edges and causes halo artifacts along object boundaries, as shown in Fig. 9(b). In Fig. 9(c), the fuzzy segmentation enables the transmission to preserve edges well along the object boundaries and greatly reduce the mismatches, resulting in a significant prevention of halo artifacts.

Fig. 10 compares halo artifact reductions by the guided filter refinement and the proposed fuzzy segmentation method. The DCP without refinement causes halo artifacts to occur along the tree branch boundaries. The refinement by a guided filter spreads the halo artifacts away to be less apparent but it does not remove them. Unlike refinement processes, the proposed fuzzy segmentation method significantly eliminates the halo artifacts.

(a) (b) (c)

Fig. 9. Halo artifacts in the dehazed images. (a) Original hazy images, (b) CEP transmission map without embedding fuzzy segmentation and its dehazing result, and (c) CEP transmission map with embedding fuzzy segmentation and its dehazing result.

(a) (b) (c) (d)

Fig. 10. Halo artifacts in the dehazed images and transmission maps. (a) Original hazy image, (b) image dehazed by the DCP with no refinement, (c) by the DCP with guided filter refinement, and (d) by the proposed CEP with the fuzzy segmentation.

C. Fast Implementation of CEP

To avoid computing the color component channels separately, we first determine the color channel having the minimum component of vectors in the color ellipsoid, c^*, that is, $c^* = \underset{c\in\{r,g,b\}}{\operatorname{argmin}}\{\hat{\mu}_{c,i} - \hat{\sigma}_{c,i}\}$. Then, Eq. (12) is rewritten as follows:

$$\begin{aligned} t_i &= 1 - \alpha \min_{c\in\{r,g,b\}} \left\{\hat{\mu}_{c,i} - \hat{\sigma}_{c,i}\right\} \\ &= 1 - \alpha \left(\hat{\mu}_{c^*,i} - \hat{\sigma}_{c^*,i}\right). \end{aligned} \tag{13}$$

The pixel colors at small patches tend to be monochromatic, as observed in [6]. Therefore, in a patch, the minimum color components of pixels are highly probably from the same color channel, indicating that the minimum component channels of each pixel are mostly the same as c^*. Then, the fast implementation of the CEP can be realized as follows:

$$\begin{aligned} \hat{\mu}_{c^*,i} &= \sum_{j\in\omega_i} P_{ij}\bar{x}_{c^*,j} \simeq \sum_{j\in\omega_i} P_{ij} \min_{c\in\{r,g,b\}} \bar{x}_{c,j}, \\ \hat{\sigma}^2_{c^*,i} &= \sum_{j\in\omega_i} P_{ij}(\bar{x}_{c^*,j} - \hat{\mu}_{c^*,i})^2 \\ &\simeq \sum_{j\in\omega_i} P_{ij} \left(\min_{c\in\{r,g,b\}} \bar{x}_{c,j} - \hat{\mu}_{c^*,i}\right)^2. \end{aligned} \tag{14}$$

To confirm the accuracy of the approximation, we tested approximately 100 naturally hazy images collected from the dataset by [6] and our own dataset. The differences in the transmission values determined by the fast implementation in (13) and by the implementation in (12) are on average less than 3%. The fast implementation reduces the complexity of computation by approximately three times, and rarely degrades the dehazing results. The pseudo code of the fast CEP implementation is in Table I.

IV. Experiments and Discussion

We evaluate the existing competitive methods and the proposed method on the image dataset [20] that has been widely used. We perform both qualitative and quantitative evaluation for natural images while doing quantitative evaluation for synthetic images. The quantitative evaluations for natural images are assessed by the measurement of image quality and those for synthetic images are oriented to measure the dehazing accuracies. We empirically fix the overall dehazing weight α at 0.95 and set the patch sizes at 15×15. These parameter values are also used widely in image dehazing and processing methods [2], [4], [21]. We implemented the fast CEP. More results are available at [22].

A. Qualitative Evaluations

Fig. 11 compares the dehazed 'Forest' image and transmission maps from the proposed CEP, the DCP [2], the color-line [6], and the haze-line [9]. For the in-depth discussion, we specify three areas: a weakly hazy area (Area A), a deep forest area with dense haze (Area B), and the area in which thin tree branches and leaves are overlaid by dense haze (Area C).

In Area A, the transmission values descend in order of the DCP, the CEP, the color-line method, and the haze-line method; and the dehazing performance strengths ascend in the same order. As the transmission values indicate, the haze-line method provides the strongest dehazing. The transmission values and the dehazing results from the CEP and the color-line method appear similar. Compared to other methods, the DCP results in insufficient dehazing because the pixels corresponding to the thin and dark branches make the transmission values large even though there are relatively few of these pixels.

In Area B, because the haze is dense and there are not irregular pixels, the prior vectors by the CEP and the DCP are almost the same, so these methods reasonably reduce the dense haze. Meanwhile, the color-line and the haze-line methods produce insufficient dehazing. As seen in the transmission map, the color-line method invalidates the transmission values in this area and interpolates the values from surrounding areas, such as the sky or ground, causing the values not to be too

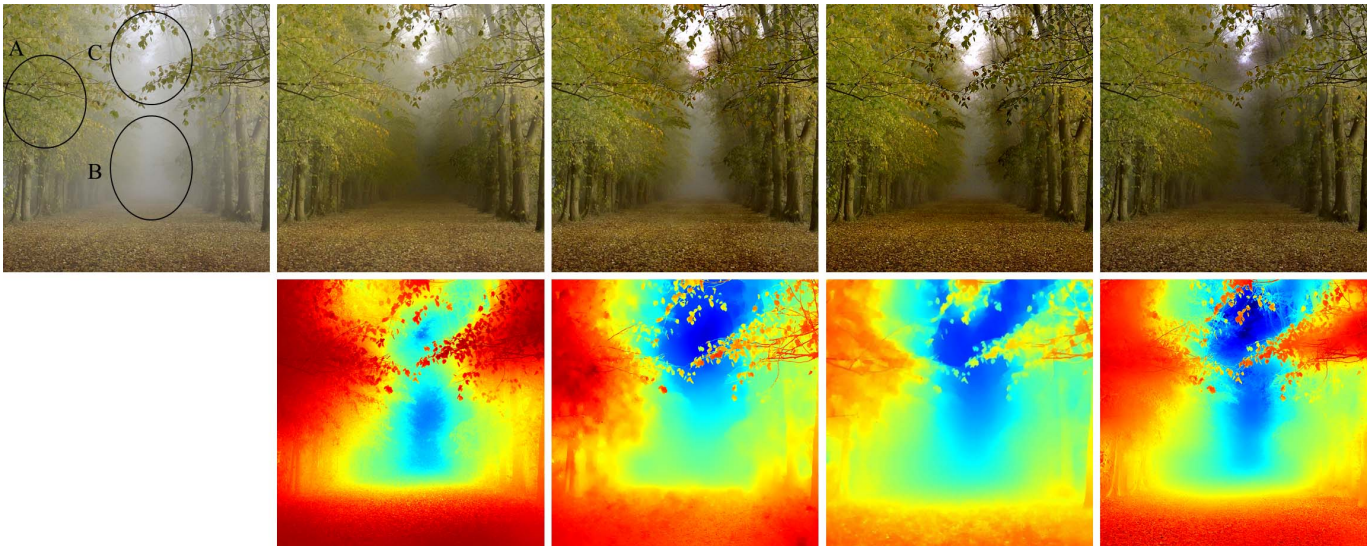

Fig. 11. Comparison of dehazed 'Forest' images and transmission maps. (a) Original image, (b) images dehazed by the DCP, (c) by the color-line, (d) by the haze-line, and (e) the proposed CEP.

small to dehaze the area effectively. Since haze-free pixels do not exist in Area B, the prior vector selected by the haze-line method is close to atmospheric light, making the transmission value large and prohibiting the method from fully reducing the dense haze. The CEP and the DCP generate transmission maps that distinguish Area B and the surrounding tree regions, whereas the maps generated by the color-line method and the haze-line method rarely outline the deep forest region. From these results, the CEP renders more of the forest in the dehazed images, compared to the other methods.

In Area C, the DCP does not fully reduce the haze for the same reason as in Area A. The color-line and haze-line methods significantly reduce the haze, but they also erode the tree leaves diluted by the dense haze. The erroneous results occur because the color lines are confused with the atmospheric light, and the cluster classification could not form the obvious haze lines. The same phenomenon occurs in the regions including the thin tree stems or small objects overlaid by strong haze, and the thin or small objects appear unnaturally wide. Meanwhile, the CEP embedding the fuzzy segmentation process reduces the haze as much as other methods while making the leaves more visible.

Fig. 12 also compares the dehazed images of 'Manhattan', 'Tree', and 'Swan' and shows the transmission map generated by the CEP. As with the Forest image, the overall dehazing strengths ascend in the order of the DCP, the CEP, the color-line method and the haze-line method. It is also observed that the strengths of the CEP and the color-line method are approximately equivalent. The DCP performs for any degree of haze, but its dehazing strengths are weak, and thin hazes usually remain along object boundaries or thin tree stems, indicating that the method is affected by the irregular small dark spots. In medium hazy areas such as the middle and bottom parts of 'Manhattan', the color-line and haze-line methods revive the natural haze-free details. However, in the heavy haze areas, such as the middle parts of 'Tree' and 'Swan', neither method sufficiently removes the haze. Reviewing the artifacts, the color-line and the haze-line methods erode and clip the heavily hazed faraway island of 'Manhattan' and also result in over-saturation that widens the thin and long stems of 'Tree'. In contrast to the other methods, the CEP produces balanced and sufficient dehazing performances in all of the images without causing apparent artifacts. However, the proposed CEP is also subject to the inherent tradeoff between maintaining color fidelity and sufficient dehazing.

B. Quantitative Evaluations

To quantitatively evaluate performances for natural images, we focus on the image quality improvement possibly measured by the ratios of newly visible edges, the restored gradient magnitudes, and the statured pixels, as devised in [23]. Table II lists the measured scores of each method. The ratios of newly visible edges show that the proposed CEP recovers more edges to be visible compared to other methods. While the color-line and haze-line methods recover more edges in most of the images, the proposed method and the DCP do for all test images. Even in 'Manhattan', the color-line and the haze-line produce negative scores, implying that the methods remove some visible edges. The gradient ratios denote that the contrast improvements are achieved in descending order of the color-line, the haze-line, the proposed CEP, and the DCP. However, score differences among the color-line method, the haze-line method, and the proposed CEP are relatively small, indicating that these methods produce comparable contrast improvements. Saturated pixel percentages verify that the DCP and proposed CEP method significantly prevents saturated pixels compared to other methods. Overall, the quality improvement scores indicate that the proposed CEP achieves the most balanced tradeoff between color fidelity maintenance and dehazing strength.

Fig. 12. Original images ('Mahattan', 'Tree', 'Swan') and their dehazed images. (a) Original images, (b) images dehazed by the DCP, (c) by the color-line, (d) by the haze-line and (e) by the proposed CEP. (f) Transmission maps by the proposed CEP.

TABLE II
QUALITY IMPROVEMENT SCORES OF DEHAZED IMAGES. RATIO OF NEWLY VISIBLE EDGES (VIS. EDGE), MEAN RATIO OF THE VISIBLE EDGE GRADIENTS (GRAD. RATIO), AND PERCENTAGE OF SATURATED PIXELS (SAT. PIXELS)

Image	DCP [2]	Color-line [6]	Haze-line [9]	CEP
Forest				
Vis. Edge	0.28	0.32	0.30	0.41
Grad. Ratio	1.37	1.57	1.59	1.54
Sat. Pixels(%)	0.02	0.09	0.51	0.00
Mahattan				
Vis. Edge	0.04	-0.11	-0.04	0.06
Grad. Ratio	1.39	1.78	1.41	1.55
Sat. Pixels(%)	0.00	0.42	4.30	0.00
Tree				
Vis. Edge	1.42	2.07	1.82	2.99
Grad. Ratio	2.19	3.76	2.64	3.35
Sat. Pixels(%)	0.00	0.00	0.08	0.00
Swan				
Vis. Edge	0.42	0.66	0.74	0.84
Grad. Ratio	2.16	3.27	3.12	2.51
Sat. Pixels(%)	0.25	6.09	0.15	0.30

Because the dataset provides natural haze-free images, the dehazing performances can be measured as the mean absolute difference (MAD) between dehazed images and natural haze-free images [20]. The hazy images were synthesized to various haze levels by varying the scattering coefficient. The additive zeros and mean Gaussian noises were also added independently to each color component.

Table III lists the MADs of dehazed images and transmission maps at low, medium, and high haze levels. The DCP is not as accurate at low and medium haze levels as the other methods, but its accuracy improves for higher haze levels. Therefore, at high haze levels, the DCP is much better than the haze-line method and almost comparable to the CEP and the color-line methods. The CEP, the color-line method, and the haze-line method yield similar accuracies at the medium haze level. The accuracy of the haze-line method drops at low and high haze levels, reaching its lowest at the high haze level. Although the CEP and the color-line methods work effectively at all haze levels, the CEP is more accurate than the color-line method at the high haze level. Fig. 13 presents the dehazed images from the high haze level.

Table IV compares the MADs at different noise levels. The DCP is not generally robust to noise because its transmission values may be obtained from irregular noisy pixels. In the small noise degree range, the accuracies of the CEP, the color-line method, and the haze-line method are not significantly different. However, as the noise degree increases, the accuracies of the color-line and haze-line methods deteriorate much more than that of the CEP. As the noise degree increases, the monochromatic assumption made by the color-line method

TABLE III

MAD SCORES OF IMAGES DEHAZED BY EACH METHOD IN DIFFERENT SCATTERING SCENES. TRANSMISSION MAD/ DEHAZED IMAGE MAD

Scattering	DCP [2]	Color-line [6]	Haze-line [9]	CEP
Road1				
low	0.122/0.046	0.075/**0.026**	0.087/0.029	**0.073**/0.031
medium	0.097/0.052	0.070/0.034	**0.055**/**0.031**	0.069/0.038
high	0.055/0.064	0.043/0.041	0.246/0.136	**0.042**/**0.039**
Lawn1				
low	0.158/0.066	**0.040**/**0.037**	0.061/0.049	0.052/0.043
medium	0.118/0.063	0.076/0.042	**0.056**/**0.031**	0.071/0.046
high	0.064/0.070	0.050/0.052	0.272/0.119	**0.045**/**0.048**
Masion				
low	0.108/0.044	**0.040**/**0.026**	0.070/0.042	0.057/0.032
medium	0.074/0.043	0.042/**0.033**	0.072/0.050	**0.039**/0.037
high	0.039/0.047	**0.029**/0.043	0.181/0.107	0.031/**0.042**
Church				
low	0.148/0.061	**0.045**/**0.029**	0.083/0.049	0.053/0.032
medium	0.070/0.048	0.036/0.034	**0.032**/**0.021**	0.039/0.035
high	0.027/0.047	**0.023**/0.039	0.211/0.146	0.024/**0.037**
Reindeer				
low	0.150/0.067	**0.057**/**0.044**	0.083/0.068	0.065/0.047
medium	0.126/0.068	0.067/0.053	0.073/0.057	**0.059**/**0.052**
high	0.072/0.070	0.053/0.063	0.235/0.293	**0.048**/**0.059**

TABLE IV

MAD SCORES OF IMAGES DEHAZED BY EACH METHOD IN DIFFERENT NOISE LEVEL SCENES. TRANSMISSION MAD/ DEHAZED IMAGE MAD

Noise power	DCP [2]	Color-line [6]	Haze-line [9]	CEP
Road1				
0.01	0.100/0.065	0.068/**0.053**	**0.061**/0.058	0.070/0.056
0.025	0.106/0.082	0.084/0.079	**0.072**/0.075	0.074/**0.071**
0.05	0.136/0.094	0.120/0.102	0.091/0.097	**0.085**/**0.082**
Lawn1				
0.01	0.116/0.051	0.056/0.041	**0.032**/**0.040**	0.056/0.052
0.025	0.109/0.071	0.056/0.068	**0.052**/**0.063**	0.065/0.071
0.05	0.115/0.093	0.114/0.105	0.099/0.095	**0.80**/**0.085**
Masion				
0.01	0.067/0.048	**0.048**/**0.036**	0.088/0.056	0.058/0.046
0.025	0.057/0.061	0.065/0.067	0.104/0.082	**0.061**/**0.064**
0.05	0.083/0.077	0.081/0.085	0.116/0.097	**0.077**/**0.079**
Church				
0.01	0.067/0.065	0.053/0.058	0.049/0.052	**0.045**/**0.047**
0.025	0.058/0.078	0.089/0.086	**0.047**/0.064	0.048/**0.058**
0.05	0.087/0.100	0.121/0.113	**0.043**/0.091	0.063/**0.076**
Reindeer				
0.01	0.119/0.063	0.077/0.049	0.093/0.053	**0.075**/**0.044**
0.025	0.109/0.068	0.084/0.062	0.104/0.070	**0.079**/**0.058**
0.05	0.117/0.083	0.106/0.094	0.131/0.096	**0.086**/**0.082**

Fig. 13. Dehazed images at high haze level.

Fig. 14. Dehazed images at high noise level.

becomes less reliable. The accuracy of the haze-line method is also unstable at the high noise level because the haze-free assumed pixels assigned as the prior vectors are more possibly corrupted by the higher noise. In contrast, the CEP uses statistical averages to calculate the transmission values and so is stable even at high noise levels. Fig. 14 shows the dehazed images from the high noise level.

From this quantitative analysis, it can be concluded that the proposed CEP performs competitively at all haze and noise levels. In particular, the method exhibits the lowest errors in most of the images from high haze and noise levels.

C. Complexity Evaluation

Table V compares the runtimes of various methods. We executed the published haze-line code [9], and directly referenced the execution times of the color-line method [6]. In order to implement the DCP, we strictly followed the procedures and parameters given in [2], with the guided filter for refining the DCP transmission map in [10]. The runtimes were normalized per pixel. The fast CEP was implemented as in Table I.

As seen in the Table, the CEP requires the least runtime. This fast execution is attributed to the following characteristics: Instead of using a post-refinement process, the method

TABLE V
AVERAGE RUNTIME OF EACH DEHAZING METHODS. PROGRAMMING LANGUAGES - M: MATLAB, C: C/C++. THE AVERAGE RUNTIME IS TESTED ON USING CORE i7 3.0 GHz PROCESSOR AND 8GB RAM

Methods	Code	Runtime(s/Mp)
DCP [2]	C	57
Fast DCP [10]	C	0.5
Color-line [6]	C	5.4
Fast color-line [6]	C	0.55
Haze-line [9]	M	5.2
CEP	C	0.35
Fast CEP	C	**0.12**

embeds the fuzzy segmentation filter into the transmission estimation process so that it can simultaneously execute the refinement process and the transmission estimation. In addition, the CEP calculates the average values rather than sorting or classifying pixel values. Considering that sorting and classifying usually require significantly more time, the CEP is reasonably expected to run faster than other methods that use classification or sorting.

V. CONCLUSIONS

We construct a statistical color ellipsoid to fit a haze pixel cluster in RGB space and then calculate the prior vector using ellipsoid geometry. The prior vector selected by the proposed method is the vector having the minimum color component on the ellipsoid surface. Combined with the statistical robustness established using average values to construct the ellipsoid, the minimum color component makes it possible for the proposed method to maximize the contrast of dehazed pixels at any haze or noise level and significantly reduce over-saturated pixels and unnatural artifacts. In addition, in order to prevent any visible halo artifact, we integrate a fuzzy segmentation process with the construction of the color ellipsoid, and thus significantly reduce the computational complexity compared to existing refinement processes.

REFERENCES

[1] R. Fattal, "Single image dehazing," *ACM Trans. Graph.*, vol. 27, no. 3, p. 72, Aug. 2008.

[2] K. He, J. Sun, and X. Tang, "Single image haze removal using dark channel prior," *IEEE Trans. Pattern Anal. Mach. Intell.*, vol. 33, no. 12, pp. 2341–2353, Dec. 2011.

[3] K. B. Gibson, D. T. Vo, and T. Q. Nguyen, "An investigation of dehazing effects on image and video coding," *IEEE Trans. Image Process.*, vol. 21, no. 2, pp. 662–673, Feb. 2012.

[4] K. B. Gibson and T. Q. Nguyen, "An analysis of single image defogging methods using a color ellipsoid framework," *EURASIP J. Image Video Process.*, vol. 2013, p. 37, Dec. 2013.

[5] G. Meng, Y. Wang, J. Duan, S. Xiang, and C. Pan, "Efficient image dehazing with boundary constraint and contextual regularization," in *Proc. IEEE Int. Conf. Comput. Vis.*, Dec. 2013, pp. 617–624.

[6] R. Fattal, "Dehazing using color-lines," *ACM Trans. Graph*, vol. 34, no. 1, 2014, Art. no 13.

[7] K. Tang, J. Yang, and J. Wang, "Investigating haze-relevant features in a learning framework for image dehazing," in *Proc. IEEE Conf. Comput. Vis. Pattern Recognit.*, Jun. 2014, pp. 2995–3000.

[8] B. Cai, X. Xu, K. Jia, C. Qing, and D. Tao, "DehazeNet: An end-to-end system for single image haze removal," *IEEE Trans. Image Process.*, vol. 25, no. 11, pp. 5187–5198, Nov. 2016.

[9] D. Berman, T. Treibitz, and S. Avidan, "Non-local image dehazing," in *Proc. IEEE Conf. Comput. Vis. Pattern Recognit.*, Jun. 2016, pp. 1674–1682.

[10] K. He, J. Sun, and X. Tang, "Guided image filtering," *IEEE Trans. Pattern Anal. Mach. Intell.*, vol. 35, no. 6, pp. 1397–1409, Jun. 2013.

[11] Y. Li, S. You, M. S. Brown, and R. T. Tan. (Jul. 2016). "Haze visibility enhancement: A survey and quantitative benchmarking." [Online]. Available: https://arxiv.org/abs/1607.06235

[12] J.-P. Tarel and N. Hautière, "Fast visibility restoration from a single color or gray level image," in *Proc. IEEE Int. Conf. Comput. Vis.*, Sep./Oct. 2009, pp. 2201–2208.

[13] C. O. Ancuti and C. Ancuti, "Single image dehazing by multi-scale fusion," *IEEE Trans. Image Process.*, vol. 22, no. 8, pp. 3271–3282, Aug. 2013.

[14] J. Huang and D. Mumford, "Statistics of natural images and models," in *Proc. IEEE Comput. Soc. Conf. Comput. Vis. Pattern Recognit.*, vol. 1. Jun. 1999, pp. 541–547.

[15] A. Lee, D. Mumford, and J. Huang, "Occlusion models for natural images: A statistical study of a scale-invariant dead leaves model," *Int. J. Comput. Vis.*, vol. 41, nos. 1–2, pp. 35–59, 2001.

[16] W.-J. Kuo and R.-F. Chang, "Approximating the statistical distribution of color histogram for content-based image retrieval," in *Proc. IEEE ICASSP*, vol. 4. Jun. 2000, pp. 2007–2010.

[17] R. M. Haralick and L. G. Shapiro, *Computer and Robot Vision*. Reading, MA, USA: Addison-Wesley, 1992.

[18] T. M. Bui, H. N. Tran, W. Kim, and S. Kim, "Segmenting dark channel prior in single image dehazing," *Electron. Lett.*, vol. 50, no. 7, pp. 516–518, Mar. 2014.

[19] C. Tomasi and R. Manduchi, "Bilateral filtering for gray and color images," in *Proc. Conf. Comput. Vis.*, Jan. 1998, pp. 839–846.

[20] R. Fattal. (2014). *Dehzaing Using Color-Lines Results and Comparisons*. [Online]. Available: http://www.cs.huji.ac.il/~raananf/projects/dehaze_cl/results/

[21] H. Oh and W. Kim, "Video processing for human perceptual visual quality-oriented video coding," *IEEE Trans. Image Process.*, vol. 22, no. 4, pp. 1526–1535, Apr. 2013.

[22] T. M. Bui and W. Kim. (2017). *Dehazing Results Using Color Ellipsoid Prior*. [Online]. Available: https://github.com/mtbui2010.CEP/

[23] N. Hautière, J.-P. Tarel, D. Aubert, and É. Dumont, "Blind contrast enhancement assessment by gradient ratioing at visible edges," *Image Anal. Stereol. J.*, vol. 27, no. 2, pp. 87–95, Jun. 2008.

Trung Minh Bui (S'17) received the B.S. degree in electronic engineering from the Ho Chi Minh City University of Technology, Ho Chi Minh city, Vietnam, in 2010. He received the M.S. degree in electronic engineering from Kyung Hee University, Yongin, South Korea, in 2014, where he is currently pursuing the Ph.D. degree. His research interests include image and video processing, computer vision, and artificial intelligence.

Wonha Kim (M'98–SM'10) received the B.S. degree in electronic engineering from Yonsei University, Seoul, South Korea, in 1985, and the M.S. and the Ph.D. degrees in electrical engineering from the University of Wisconsin–Madison, USA, in 1988 and 1997, respectively. From 1997 to 2000, he was with the Los Alamos National Laboratory, Los Alamos, NM, USA, as a Software Engineer. From 2000 to 2003, he was with the Division of Electronics, Information and Communication Engineering, Myongji University, Yongin, South Korea, as an Assistant Professor. He was a Visiting Scholar with the University of California, San Diego, from 2009 to 2010. He is currently a Professor with the College of Electronics and Information Engineering, Kyung Hee University, Yongin. His research interests include image and video coding and processing, color vision, and 2D/3D vision processing.